

Effective 2D thickness for the Berezinskii-Kosterlitz-Thouless-like transition in a highly underdoped $\text{La}_{2-x}\text{Sr}_x\text{CuO}_4$

P. G. Baity,^{1,2} Xiaoyan Shi,^{1,2,*} Zhenzhong Shi,¹ L. Benfatto,³ and Dragana Popović^{1,2,†}

¹*National High Magnetic Field Laboratory, Florida State University, Tallahassee, Florida 32310, USA*

²*Department of Physics, Florida State University, Tallahassee, Florida 32306, USA*

³*ISC-CNR and Dept. of Physics, Sapienza University of Rome, P.le A. Moro 5, 00185, Rome, Italy*

(Dated: January 26, 2016)

The nature of the superconducting transition in highly underdoped thick films of $\text{La}_{2-x}\text{Sr}_x\text{CuO}_4$ ($x = 0.07$ and 0.08) has been investigated using the in-plane transport measurements. The contribution of superconducting fluctuations to the conductivity in zero magnetic field, or paraconductivity, was determined from the magnetoresistance measured in fields applied perpendicular to the CuO_2 planes. Both the temperature dependence of the paraconductivity above the transition and the nonlinear current-voltage ($I - V$) characteristics measured across it, exhibit the main signatures of the Berezinskii-Kosterlitz-Thouless (BKT) transition. The quantitative comparison of the superfluid stiffness, extracted from the $I - V$ data, with the renormalization-group results for the BKT theory, reveals a large value of the vortex-core energy. This finding is confirmed by the analysis of the paraconductivity obtained using different methods. The results strongly suggest that the characteristic energy scale controlling the BKT behavior in this layered system corresponds to the superfluid stiffness of a few layers.

PACS numbers: 74.40.-n, 74.72.Gh, 74.62.En

I. INTRODUCTION

One of the most intriguing phenomena in condensed matter systems is the occurrence of the so-called Berezinskii-Kosterlitz-Thouless¹⁻³ (BKT) transition in two-dimensional (2D) superfluid systems. The main ingredients of the BKT physics were described originally within the context of the two-dimensional XY model, which is an effective model for the collective phase of the superfluid order parameter.^{4,5} Here logarithmically interacting vortex-like topological excitations drive the transition from the superfluid state, where they are bound together in vortex-antivortex (V-AV) pairs, to the metallic one, where single vortex excitations proliferate. This mechanism leads in principle to several peculiar signatures in the physical observables, such as the universal and discontinuous jump⁶ of the superfluid density at T_{BKT} , the observation of which in ^4He films⁷ was the first experimental proof of the existence of a BKT transition. Afterwards, interest in BKT physics was triggered mainly by the possibility to observe it in superconducting (SC) systems that can be considered to be in the 2D limit. On very general grounds, this occurs for systems with low superfluid stiffness J_s , defined as the energy scale associated to the areal density of superfluid electrons:

$$J_s = \frac{\hbar^2 n_s d_{BKT}}{4m} = \frac{\hbar^2 c^2}{16\pi e^2} \frac{d_{BKT}}{\lambda^2}, \quad (1)$$

where n_s, m denote the superfluid density and mass of the carriers, respectively, λ is the magnetic penetration depth and d_{BKT} denotes a transverse length scale over which the system can be seen as effectively 2D. The possibility to see BKT physics is connected to a low value of d_{BKT}/λ^2 : indeed, despite the presence of screening supercurrents, the interaction between vortices remains log-

arithmic when the Pearl screening length $\Lambda = 2\lambda^2/d_{BKT}$ overcomes the system size.⁸ In addition, since the distance between T_{BKT} and the ordinary BCS temperature T_c scales as $(T_c - T_{BKT})/T_c \propto T_{BKT}/J_s$, a clear BKT regime can only be identified when J_s gets reduced. In films of conventional superconductors, these conditions are usually realized when the film thickness d is reduced. In those cases, by identifying d_{BKT} with d , typical BKT signatures have been observed⁹⁻¹⁶ by means of different experimental probes. The universal jump of the superfluid density has been seen either via direct measurements of the inverse penetration depth^{9-14,16} or via a discontinuous jump of the exponent of the nonlinear $I - V$ characteristics.⁹ At the same time, the vortex proliferation above T_{BKT} has been identified^{9,14,15} from an exponential divergence of the correlation length above T_{BKT} , which leads to a peculiar paraconductivity above the transition.^{4,17}

An alternative route for the observation of BKT physics is presented by *bulk* layered systems, in which the magnetic-field distribution of a vortex differs drastically from the monopole-like Pearl solution in uniform films:^{4,18} the presence of other superconducting layers squeezes the field of a pancake vortex into a narrow strip of size λ along the c axis. This in turn implies that the logarithmic dependence of the interaction potential between two vortices placed in the same layer persists up to all length scales, as in a neutral superfluid, making in principle the stack of uncoupled layers the best possible system to observe a true BKT transition, with the 2D unit in Eq. (1) corresponding to each isolated plane. In the presence of Josephson coupling between layers, the upper cut-off for the logarithmic interaction between vortices becomes^{4,18} $\Lambda_J \simeq \xi_0/\sqrt{J_\perp/J_\parallel}$, where ξ_0 is the zero-temperature in-plane coherence length, and $J_{\parallel,\perp}$ are

the in-plane and out-of-plane superfluid stiffness, respectively. If the interlayer coupling is weak, *i.e.* $J_{\perp}/J_{\parallel} \ll 1$, this length scale is large enough to allow for a BKT-like description of the vortex-antivortex interaction, independent of the film thickness d . In practice, even if the finite-size effect due to Λ_J leads to a rounding of the discontinuous jump in J_s , the analysis of anisotropic 3D XY -like model^{19–24} shows that the unbinding of vortex-antivortex pairs in each plane is still the mechanism driving the transition, in analogy with the purely 2D case. Therefore, in a weakly coupled, layered superconductor, one expects to observe a BKT-like transition at a 3D transition temperature that is slightly higher than the BKT transition temperature of a single layer of an equivalent uncoupled system.

Such a description is expected to be appropriate for underdoped samples of cuprate superconductors, which are highly anisotropic, layered materials. Here one also finds that the superfluid stiffness is suppressed by the proximity to the Mott insulator,^{25,26} making the separation between T_{BKT} and T_c large, while avoiding the additional consequences of an increase of the disorder level, as it occurs in films of conventional superconductors when the thickness is reduced. According to this argument, in bulk samples of underdoped cuprates one should be able to identify BKT signatures assuming that the fundamental 2D unit is represented by isolated CuO_2 layers, *i.e.* the transverse length scale d_{BKT} in Eq. (1) would coincide with the interlayer distance d_c , as pointed out in the seminal work by Emery and Kivelson.²⁵ However, it has been recently shown²³ that this picture is somehow too simplified, since one should also account for the nontrivial role of the vortex-core energy μ , which is the energetic cost needed to create the vortex at the smallest length scale ξ_0 . Indeed, even if the layers are weakly coupled, what matters for the vortex proliferation is the competition at large distances between the effective vortex fugacity and the effective Josephson coupling. As a consequence, when μ is large, the Josephson coupling between layers can prevent the vortex unbinding, moving the BKT transition away from the value expected for each isolated layer, resulting in an effective dimension d_{BKT} larger than d_c .

So far, the experimental situation in cuprate superconductors has been controversial. For example, the direct measurements of the inverse penetration depth have shown that, in the $\text{YBa}_2\text{Cu}_3\text{O}_{7-x}$ family, no BKT jump is observed even in strongly-underdoped thick films^{27,28} or crystals.²⁹ A BKT-like superfluid-density jump is only seen in few-unit-cell thick films of $\text{YBa}_2\text{Cu}_3\text{O}_{7-x}$ (Ref. 30) or $\text{Bi}_2\text{Sr}_2\text{CaCu}_2\text{O}_{8+x}$ (Ref. 31), but even in this case, as the samples get underdoped, the effective d_{BKT} seems to cross over to the sample thickness and the superfluid-density jump gets smeared out. While this can be explained indeed by an increase of the vortex-core energy with underdoping,³² one should notice that the simultaneous appearance of an anomalously large dissipative response suggests that spurious finite-frequency

effects can also be present, as emphasized recently in the analysis of thin films of NbN.³³ These spurious effects are instead absent in the dc measurements of the $I - V$ exponent that suggested a BKT-like jump very near T_c in cuprate samples.^{34–38} However, this measurement allows one to extract directly the effective 2D areal stiffness (1), *i.e.* the combination d_{BKT}/λ^2 , so d_{BKT} can be determined only if λ is known by measurements in similar samples. Finally, the analysis of the paraconductivity, *i.e.* of the SC fluctuations above T_c , also raises some questions on the occurrence or not of a BKT transition. Indeed, on one hand, the SC fluctuations have been proved to have a strong 2D character in several cuprate families (*e.g.* Refs. 39–43) with the typical 2D unit being identified as the distance between the CuO_2 layers d_c . On the other hand, these are ordinary Gaussian (amplitude and phase) fluctuations, with a BKT regime that, if present, is restricted to a small range of temperatures near T_c in the most underdoped samples.^{37,43}

In the present work, we address the issue of the identification of the scale d_{BKT} in cuprate superconductors by making a simultaneous analysis of the BKT signatures both below and above T_{BKT} in two highly underdoped samples of $\text{La}_{2-x}\text{Sr}_x\text{CuO}_4$. We first extract the paraconductivity above T_{BKT} (Sec. II B), and then determine the temperature dependence of the anomalous 2D exponent of the $I - V$ characteristics across it (Sec. II C). In Sec. III A, the direct comparison of the experimental $I - V$ data with the renormalization-group results for the BKT theory allows us to extract a large value of the vortex-core energy μ , consistent with that obtained from the analysis of paraconductivity in Sec. II B. According to earlier theoretical work,^{23,32} the large value of μ obtained in our study corresponds to $d_{BKT} \simeq (2 - 3)d_c$. Furthermore, this value of the vortex-core energy can be used to reduce considerably the fitting parameters in the well-known Halperin-Nelson formula⁴⁴ for the paraconductivity above T_{BKT} , spanning both the BKT and Aslamazov-Larkin^{45–47} (AL) regimes of the SC fluctuations. This analysis (Sec. III B) confirms that the effective length scale d_{BKT} is a few times larger than d_c , in agreement with the expectation^{23,32} for a layered weakly-coupled system with a large vortex-core energy. Our study clarifies how different transverse length scales enter in the analysis of the SC fluctuations above and below T_{BKT} , solving the apparent contradiction between previous measurements.

II. EXPERIMENTS

A. Samples and measurement techniques

The samples were $\text{La}_{2-x}\text{Sr}_x\text{CuO}_4$ (LSCO) films with the nominal doping $x = 0.07$ and $x = 0.08$. They were patterned into standard Hall bars with the length $L = 2.0$ mm and the width $W = 0.3$ mm; the distance between voltage contacts was 1.01 mm. The films were

75 unit cells (150 CuO₂ layers) thick ($d \approx 1000$ Å) and grown by molecular beam epitaxy. The films and samples were described in detail elsewhere.⁴⁸ The samples become superconductors below the temperature $T_{R=0}(x)$, defined as the temperature at which the in-plane resistance R becomes zero. The measured $T_{R=0}$ were (3.9 ± 0.1) K and (9.7 ± 0.3) K for samples $x = 0.07$ and 0.08 , respectively.

The in-plane sample resistance and magnetoresistance were measured in ³He cryostats (base $T \approx 0.25$ K) with a standard four-probe ac method (~ 13 -16 Hz) in the Ohmic regime, using either SR7265 lock-in amplifiers or a LR-700 resistance bridge. The magnetic fields H up to 18 T were applied perpendicular to CuO₂ planes ($H \parallel c$ axis) and swept at constant temperatures. The sweep rates of 0.02-1 T/min were low enough to avoid the heating of the sample from eddy currents.

The current-voltage (I - V) measurements were carried out at constant temperatures (T) in $H = 0$ using ³He and variable-temperature insert (base $T \approx 1.3$ K) cryostats. DC square pulses provided by a Keithley 6221 current source were applied to the samples, while a Keithley 2182A nanovoltmeter measured the voltage response. Each data point on the I - V curve was found by averaging measurements with positive and negative pulse polarities. Such a four-point dc method⁴⁹ avoids possible effects of parasitic capacitances (*e.g.* from the sample contacts) and obviates Joule heating, while retaining the increased sensitivity of a finite-frequency technique and eliminating the effects of thermal electromotive forces. Current excitations between 50 nA and 1 mA were typically used, depending on the film doping and temperature.

The addition of current noise to a device with an intrinsic nonlinear behavior can create an Ohmic response at low currents⁵⁰ and, in particular, it can create Ohmic behavior even below T_{BKT} . Therefore, for the I - V measurements, filtering was provided at room temperature by a 1.75 nF low-pass π filter in series with a 1 kΩ resistor on each lead to the sample. The π filters and the resistors were encased in a shielded box attached to the top of the cryostat probe. This filter box provided a 5 dB (60 dB) noise reduction at 10 MHz (1 GHz), which enabled the observation of nonlinear I - V behavior at low excitations amid masking current noise.

B. High-field magnetoresistance measurements and superconducting fluctuations

By approaching the superconducting transition from above, it is in principle possible to identify the BKT transition from the temperature dependence of the contribution of superconducting fluctuations (SCFs) to conductivity (or “paraconductivity”), $\Delta\sigma_{SCF}(T) = \rho(T)^{-1} - \rho_n(T)^{-1}$, where $\rho(T)$ and $\rho_n(T)$ are the measured and normal-state resistivity, respectively. In cuprates, the determination of $\rho_n(T)$ has been somewhat ambiguous and controversial (see, *e.g.*, Ref. 43 and references therein). We emphasize, however, that the precise determination

of (finite) ρ_n is not crucial for the extraction of $\Delta\sigma_{SCF}$ in the regime of interest, very near the BKT transition where the contribution of SCFs diverges (Eq. (3) below). On the other hand, it may introduce considerable errors into the values of $\Delta\sigma_{SCF}$ far from it.⁴³ This issue is demonstrated and discussed further in Sec. III B.

In this Section, we adopt a method that uses transverse ($H \parallel c$) magnetoresistance measurements to determine the extent of SCFs. In particular, above a sufficiently high magnetic field $H'_c(T)$, SCFs are completely suppressed (*i.e.* they become unobservable in the experiment) and the normal state is fully restored. In the normal state, the magnetoresistance of cuprates increases as H^2 at low fields^{43,48,51-60} ($\omega_c\tau \ll 1$, where ω_c is the cyclotron frequency and τ is the scattering time), similar to the classical orbital effect in conventional metals.⁶¹

$$\frac{\rho_n(H) - \rho_n(0)}{\rho_n(0)} = (\omega_c\tau)^2 \propto H^2, \quad (2)$$

Therefore, the values of H'_c can be found from the downward deviations from such quadratic dependence that arise from SCFs when $H < H'_c$.^{43,48,56,58,59} The SCF contribution to the conductivity can be determined then as $\Delta\sigma_{SCF}(T, H) = \rho(T, H)^{-1} - \rho_n(T, H)^{-1}$, where $\rho(T, H)$ is the measured resistivity and $\rho_n(T, H)$ is obtained by extrapolating the region of H^2 magnetoresistance observed at high enough H and T . The advantages of this method^{43,56} over some of the earlier ones (*e.g.* Refs. 41 and 62) are that it does not rely on any assumptions about the T dependence of ρ_n , and it makes it possible to determine both the paraconductivity $\Delta\sigma_{SCF}(T, H = 0)$ and the SCF contribution to conductivity in the presence of magnetic field.

Figure 1(a) shows representative $\rho(H)$ curves ($H \parallel c$) obtained on the $x = 0.07$ LSCO sample. The condition for the weak-field limit is satisfied in the entire regime of interest as $\omega_c\tau \approx 0.5$ at 18 T and 5 K, where it reaches its maximum value. By tracking the gradual evolution of the magnetoresistance curves measured at different T [Fig. 1(b)], from the high- T region where the H^2 dependence is unambiguous, to lower T where SCFs are more pronounced, we were able to determine the values of the onset fields $H'_c(T)$ (see Appendix A for a more detailed discussion).

Figure 2(a) inset shows $H'_c(T)$, determined from Fig. 1(b) for the $x = 0.07$ sample and fitted by a simple quadratic expression $H'_c(T) = H'_c(0)[1 - (T/T_2)^2]$, similar to earlier studies.^{43,48,56,58,59} In zero field, SCFs become observable below $T_2 = 29$ K. In Sec. III B, we show explicitly that the exact determination of ρ_n , and thus the determinations of $H'_c(T)$ and T_2 , does not affect our conclusions. Hereafter we focus only on the zero-field behavior.

Figure 2(a) shows that $\Delta\sigma_{SCF}(H = 0)/\sigma_n(H = 0)$, where $\sigma_n = 1/\rho_n$, increases by several orders of magnitude as temperature is reduced towards $T_{R=0} \approx 4$ K, reminiscent of the exponential divergence expected at the BKT transition. Indeed, in 2D the paraconductivity can

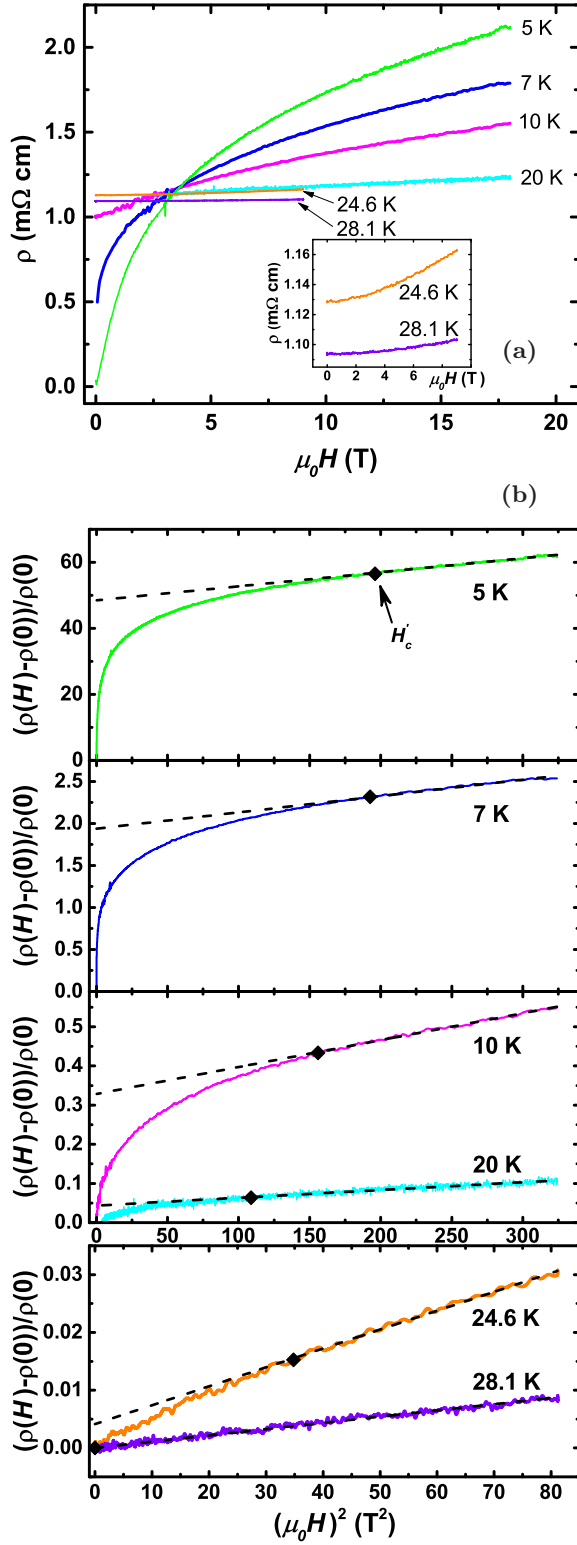


FIG. 1. (Color online) $x = 0.07$ LSCO film. (a) Resistivity *vs.* transverse magnetic field ($H \parallel c$) up to 18 T for different T , as shown. The highest T data are also shown in the inset for clarity. (b) Magnetoresistance data from (a) plotted *vs.* H^2 . Symbols (black diamonds) show $H'_c(T)$, the fields above which SCFs are fully suppressed and the H^2 dependence of the normal-state resistivity ρ_n is observed. Dashed lines are linear fits representing the contributions from normal state transport, *i.e.* they correspond to $[\rho(H) - \rho(0)]/\rho(0) = [\rho_n(0) - \rho(0)]/\rho(0) + [\rho_n(0)/\rho(0)]a_{trans}H^2$.

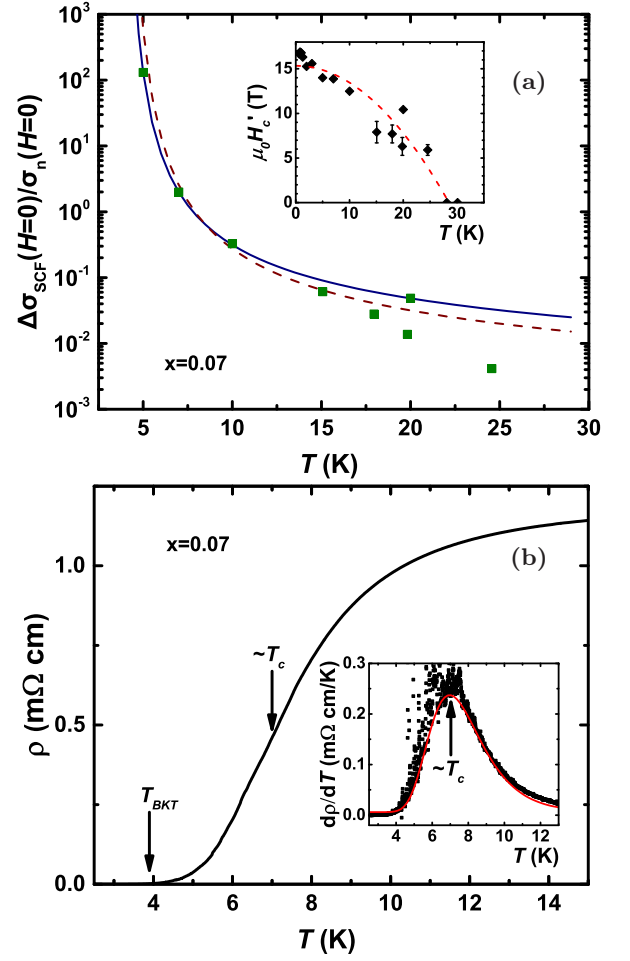


FIG. 2. (Color online) $x = 0.07$ LSCO film. (a) Symbols show $\Delta\sigma_{SCF}(T, H = 0)/\sigma_n(H = 0)$ *vs.* T , as determined from Fig. 1. The solid line is a fit to Eq. (4) with $T_{BKT} = 3.8$ K and fitting parameters $A = 17.9$, $b = 2.9$; the dashed line corresponds to $T_{BKT} = 4.0$ K, $A = 29$, $b = 3.3$. Inset: The onset field $H'_c(T)$ below which SCFs become observable. The dashed line is a fit $H'_c = H'_c(0)[1 - (T/T_2)^2]$, with $\mu_0 H'_c(0) = 15$ T and $T_2 = 29$ K. (b) ρ *vs.* T in $H = 0$. Arrows point at $T_{BKT} = T_{R=0}$ and T_c ; T_c was estimated as shown in the inset. Inset: The temperature at the inflection point of the $\rho(T)$ curve, where $d\rho/dT$ has a maximum, is taken as an estimate of T_c in the calculation of α from Eq. (5).

always be expressed as

$$\Delta\sigma_{SCF}/\sigma_n = \left[\frac{\xi(T)}{\xi_0} \right]^2, \quad (3)$$

where $\xi(T)$ is the SC correlation length, whose temperature dependence depends on the nature of the SC fluctuations. The usual Aslamazov-Larkin^{45–47} (AL) paraconductivity describes the fluctuating Cooper pairs above the mean-field temperature T_c , and leads to a power-law divergence of the coherence length $\xi^2 \sim (T - T_c)^{-1}$. In contrast, within BKT theory, $\xi^2(T) \sim 1/n_F$ measures the inverse density n_F of free vortices above T_{BKT} , and

diverges exponentially as $T \rightarrow T_{BKT}$. An interpolation formula between these two regimes was first proposed by Halperin and Nelson⁴⁴

$$\frac{\Delta\sigma_{SCF}}{\sigma_n} = \left(\frac{2}{A} \sinh \frac{b}{\sqrt{t}} \right)^2, \quad T \gtrsim T_{BKT}, \quad (4)$$

where $t = (T - T_{BKT})/T_{BKT}$, and A and b are numerical constants. More recently, a renormalization-group (RG) study⁶³ of the BKT transition showed that parameter b is strictly connected to two relevant physical quantities:

$$b \simeq 2\alpha\sqrt{t_c}, \quad \alpha = \mu/\mu_{XY}, \quad (5)$$

where t_c is the distance between the mean-field and BKT critical temperatures

$$t_c \equiv \frac{T_c - T_{BKT}}{T_{BKT}}, \quad (6)$$

while α is the vortex-core energy μ expressed in units of the conventional value μ_{XY} that it assumes in the XY model (see also Eq. (16) below). According to Eq. (3), the exponential BKT behavior is limited to the range of temperatures $t \ll t_c$, while above it, one recovers the usual AL paraconductivity.

The paraconductivity shown in Fig. 2(a) has been fitted to Eq. (4) by taking $T_{BKT} = T_{R=0} = (3.9 \pm 0.1)$ K [Fig 2(b)]. Surprisingly, it is possible to get a good fit to the data even up to very high temperatures ~ 20 K with reasonable values of A and b [*e.g.* dashed line in Fig. 2(a)]. However, within the error for T_{BKT} , the lower- T data up to ~ 10 K are described better with the fitting parameters in the range $A = 13$ – 20 and $b = 2.5$ – 3.0 [*e.g.* solid line with $A = 17.9$ and $b = 2.9$ in Fig. 2(a)]. Assuming that $T_c \sim 7$ K, *i.e.* of the order of the temperature where $d\rho/dT$ has a maximum [Fig 2(b) inset], Eq. (5) then yields enhanced values of the vortex-core energy, $\mu/\mu_{XY} \simeq 1.4$ – 1.7 , consistent with previous work.^{23,32}

The above analysis of the SCFs above a SC transition, which occurs at $T_{BKT} = T_{R=0}$, suggests the presence of a BKT fluctuation regime at $T_{BKT} < T < T_c \sim 7$ K, followed by a crossover to the AL regime at $T > T_c$. It is worth noting that the crossover to the AL regime gives some indication on the transverse length scale controlling the Gaussian fluctuations in the sample. Indeed, when $t \gg t_c$, Eq. (4) reduces to

$$\frac{\Delta\sigma_{SCF}}{\sigma_n} \simeq \frac{4b^2}{A^2} \frac{T_{BKT}}{T - T_{BKT}} \simeq \kappa_{BKT} \frac{T_c}{T - T_c}, \quad (7)$$

where, on the r.h.s., $\kappa_{BKT} \equiv 4b^2 T_{BKT}/(A^2 T_c)$ and we replaced $T - T_{BKT}$ with $\simeq T - T_c$, which is correct when T is sufficiently larger than T_c so that the difference between T_c and T_{BKT} can be neglected. We note that, in films of conventional superconductors,^{14,64} usually t_c is at most of order 0.1, so the crossover from the pure BKT behavior to the AL one occurs for relatively small reduced temperatures t . In our samples, t_c is as large as 0.7, so the asymptotic AL behavior (7) is reached at higher

temperatures. On the other hand, since the SCFs regime extends up to reduced temperatures as large as $t \sim 3$ – 4 [Fig. 2(a)], there is still a large temperature regime where the approximation (7) is valid. This expression has to be compared with the usual AL formula^{45–47} that gives

$$\frac{\Delta\sigma_{AL}}{\sigma_n} = \frac{\rho_n/d_{AL}}{16R_c} \frac{T_c}{T - T_c} \equiv \kappa_{AL} \frac{T_c}{T - T_c}, \quad (8)$$

where $R_c = \hbar/e^2 = 4.1$ k Ω . By mapping the expressions (7) and (8), we can see that the high- T limit of the interpolating HN formula also fixes the prefactor κ_{AL} that controls the strength of the AL fluctuations in the Gaussian regime at $T \geq T_c$. The latter one depends in turn on the transverse length scale d_{AL} that identifies the 2D unit for AL fluctuations [see Eq. (8)]. By using the estimates of b, A given above, we obtain that $\kappa_{BKT} = 4b^2 T_{BKT}/(A^2 T_c) \simeq 0.1$. Thus, from the measured $\rho_n \simeq 1$ m Ω cm and by matching κ_{BKT} and κ_{AL} , we conclude that d_{AL} is of the same order as the interlayer distance d_c , in full agreement with previous work in the literature.^{41,42} In other words, as far as the Cooper-pair fluctuations are concerned, the fluctuation regime displays marked 2D character with decoupled layers, consistent with the standard expectation for a weakly-coupled layered superconductor.⁴⁷ On the other hand, the BKT paraconductivity does not allow us to extract any precise information on the scale d_{BKT} controlling the vortex physics below T_{BKT} . To address this issue, and to confirm the fit based on the paraconductivity data extracted from the high-field magnetoresistance measurements [Fig. 2(a)], we analyze the $I - V$ characteristics, whose behavior is, in fact, one of the key signatures of the BKT transition.

C. Current-voltage characteristics and superfluid stiffness

The most famous hallmark of the BKT transition is observed by approaching T_{BKT} from below. In particular, the superfluid stiffness J_s , defined in Eq. (1), exhibits the so-called universal jump at the transition, *i.e.*

$$J_s(T_{BKT}^-) = \frac{2}{\pi} T_{BKT}, \quad J_s(T_{BKT}^+) = 0. \quad (9)$$

Here the T dependence of $J_s(T)$ includes both the quasi-particle excitations, which would drive J_s continuously to zero at T_c , and vortex-like phase fluctuations, which are instead responsible for the discontinuous jump (9). The latter directly influences the behavior of the exponent a in the $I - V$ characteristics:

$$V \propto I^{a(T)}, \quad a(T) = \frac{\pi J_s(T)}{T} + 1. \quad (10)$$

The superlinear behavior in Eq. (10) is due to the ability of a sufficiently large current to unbind vortex-antivortex pairs. From Eq. (9), it follows then that a should jump

from $a = 3$ at $T = T_{BKT}^-$ to $a = 1$ at $T = T_{BKT}^+$. Below T_{BKT} , the exponent a is expected to increase with decreasing T since the superfluid density increases.

The voltage-current characteristics are shown in Figs. 3(a) and 3(b) on a log-log scale for the $x = 0.07$ and $x = 0.08$ films, respectively. The power-law behavior $V \propto I^{a(T)}$ is observed at all T in the low-current limit. In that regime, the $V(I)$ dependence is thought to arise from the thermally dissociated vortex-antivortex pairs for $T > T_{BKT}$ and from current-induced dissociation for $T < T_{BKT}$. At the highest currents in Figs. 3(a) and 3(b), heating effects become important. The temperature dependent exponents $a(T)$ were determined as the slopes of the linear fits of the data at the lowest currents [Figs. 3(a) and 3(b)]. We note that, due to a large value of t_c , the fitting range, both in current and in temperature, is much wider than usual, *i.e.* compared to systems that are clearly 2D, such as interfaces⁶⁵ and films.⁶⁶ The values of $a(T)$ are presented in Fig. 3(c) for both samples. A steep change of a from its Ohmic value ($a = 1$) at high T to large values > 3 is indeed observed with decreasing T . In particular, $a(T)$ in the $x = 0.08$ sample exhibits a jump-like behavior as expected, but the $a(T)$ dependence is smoother in a more highly underdoped sample. Nevertheless, a reaches 3 at $T = (3.6 \pm 0.1)$ K and (9.4 ± 0.1) K for samples $x = 0.07$ and $x = 0.08$, respectively, close to their $T_{R=0}$ values and consistent with the assumption in Sec. II B that $T_{R=0} = T_{BKT}$.

Even though the T_{BKT} values will be determined more precisely in Sec. III A by the theoretical analysis that takes into account the smearing of the BKT jump by the presence of inhomogeneities, we can estimate the order of magnitude of $J_s(T_{BKT})$ from the temperature where $a(T) = 3$ using Eq. (9). In the $x = 0.07$ sample, for example, we have $J_s(T_{BKT} \approx 3.6 \text{ K}) \approx 2.3 \text{ K}$. Using this value and Eq. (1) expressed as⁶⁴

$$J_s[\text{K}] = 0.62 \frac{d_{BKT}[\text{\AA}]}{\lambda^2[\mu\text{m}^2]}, \quad (11)$$

we find that, if the effective transverse length scale d_{BKT} coincides with the film thickness ($\approx 10^3 \text{ \AA}$), $\lambda(T_{BKT}) \approx 16 \mu\text{m}$, while for $d_{BKT} \simeq d_c \approx 7 \text{ \AA}$ we obtain $\lambda(T_{BKT}) \approx 1.4 \mu\text{m}$. Based on the doping and temperature dependences of the penetration depth measured in similar LSCO films,⁶⁷ we estimate that $\lambda(T_{BKT})$ does not exceed a value of $2\text{--}3 \mu\text{m}$ for our $x = 0.07$ sample. Therefore, we find much better agreement between the results of our $I - V$ measurements and penetration depth studies by assuming that the *effective* sample thickness is somewhat larger than the interlayer spacing, but not as large as the whole thickness of the sample. As we shall see below, this conclusion is confirmed by a detailed comparison between $J_s(T)$ extracted from the $a(T)$ exponent and the theoretical prediction for the BKT behavior, when the non-trivial role of the vortex-core energy is taken into account.

Finally, we remark that, in our samples, we do not expect to observe the Ohmic response in the $I - V$ char-

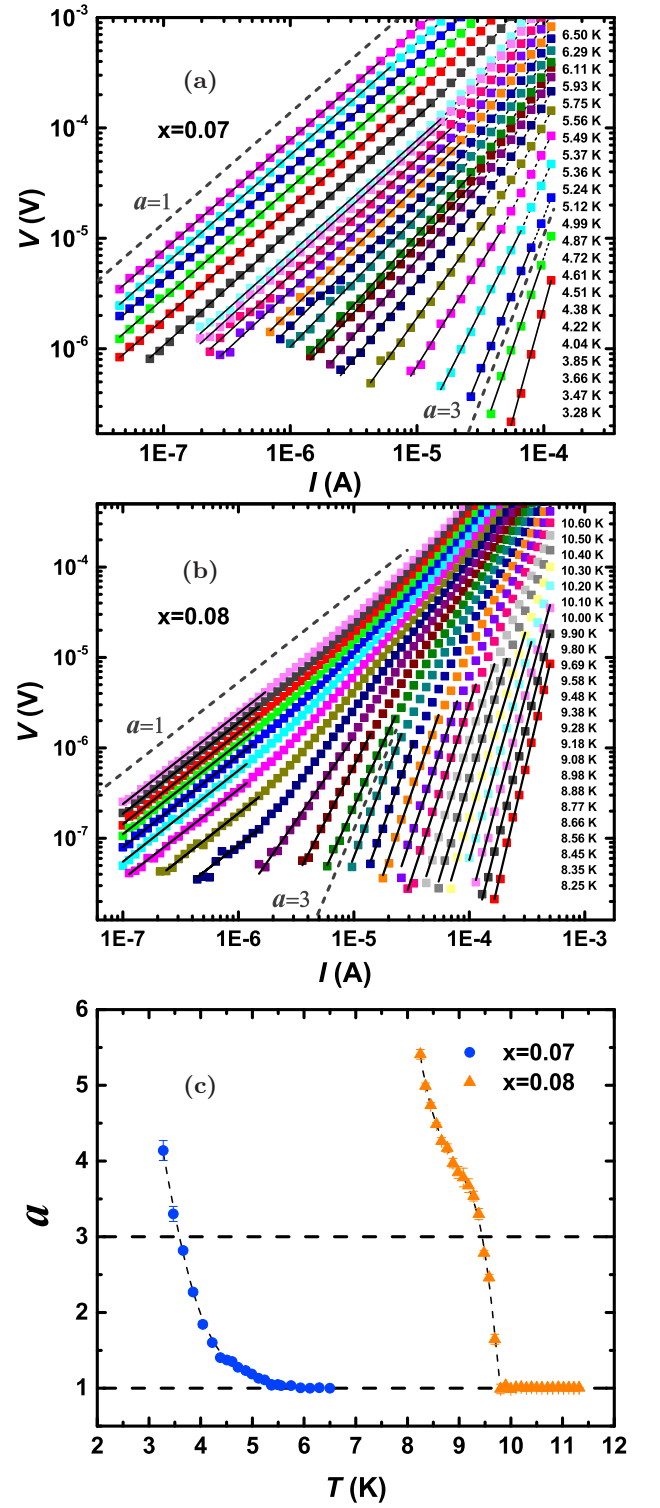


FIG. 3. (a), (b) Voltage-current characteristics on a log-log scale for $x = 0.07$ and $x = 0.08$ samples, respectively, at different T , as shown. At the lowest excitations, $V \propto I^{a(T)}$, where the solid lines are linear fits with the slopes corresponding to $a(T)$. In both panels, the dashed lines with slopes $a = 1$ and $a = 3$ guide the eye. (c) $a(T)$ for both samples. The dashed line $a = 3$ crosses the data at (3.6 ± 0.1) K and (9.4 ± 0.1) K for samples $x = 0.07$ and $x = 0.08$, respectively.

acteristics caused by finite-size effects.^{68–71} Indeed, it is known that the dc $I - V$ curves probe the contribution of dissociated vortex-antivortex pairs separated by a distance $r^* = 2\pi J_s c W / \Phi_0 I$. Therefore, at small currents, which probe r^* larger than the sample width ($W < L$), the free vortices will dominate the resistance and the $I - V$ characteristics will be Ohmic. On the other hand, the nonlinear behavior (10) of the $I - V$ characteristics can only be seen when $r^* < W$, *i.e.* above a threshold current^{4,63} I^* ,

$$I^* = \frac{2J_s \pi c}{\Phi_0} \simeq \frac{4k_B T_{BKT} c}{\Phi_0}. \quad (12)$$

By using the above estimate $T_{BKT} \approx 3.6$ K for the $x = 0.07$ sample, one gets $I^* \simeq 2.68 \times 10^{-8} (\text{A/K}) T_{BKT} [\text{K}] \sim 1 \times 10^{-7}$ A. In the presence of inhomogeneous domains of size $L' < L$, the threshold current I^* is expected⁶³ to increase with respect to the estimate (12). However, since the homogeneous value (12) we found is considerably smaller than the currents at which the measurements are performed, finite-size effects are not expected to manifest themselves in our experiment. Indeed, Figs. 3(a) and 3(b) show that, below T_{BKT} , the crossover from the nonlinear behavior (10) back to the Ohmic one is not observed even at the lowest measured current.

III. THEORETICAL ANALYSIS OF THE DATA

A. Superfluid stiffness

We extract from Eq. (10) the temperature dependence of the superfluid stiffness $J_s(T)$, which we analyze along the lines of the approach discussed earlier for both conventional^{14,33,63,64} and cuprate superconductors.^{23,32} In Eq. (10), the temperature dependence of the superfluid stiffness $J_s(T)$ is due to both quasiparticle excitations, which induce a BCS-like suppression of $J^{BCS}(T)$ at all temperatures up to T_c , and vortex-like excitations, which become relevant near $T_{BKT} < T_c$. Since our $I - V$ measurements are rather close to T_c , we can assume for $J^{BCS}(T)$ a linear behavior,

$$J^{BCS}(T) = J_0 \left(\frac{T_c - T}{T_c} \right). \quad (13)$$

The effect of vortices is taken into account by solving the BKT renormalization-group equations, whose relevant variables are

$$K = \frac{\pi J^{BCS}(T)}{T}, \quad (14)$$

$$g = 2\pi e^{-\beta\mu}, \quad (15)$$

where g is called the vortex fugacity ($\beta = 1/k_B T$). Here $J^{BCS}(T)$ determines the value of K at the shortest length scale of the problem, *i.e.* the SC coherence length ξ_0 , while the large-distance behavior will be determined by

the presence or not of free-vortex excitations, described by the large-distance behavior of the vortex fugacity. The physical superfluid stiffness J_s is then obtained by the numerical solution of the RG equations at large distances (see Appendix B for more details).

Apart from the starting value of $J^{BCS}(T)$, which can be determined by comparison with the data far from T_{BKT} , the second relevant energy scale in the problem is the ratio μ/J_s . Here we take it as a free parameter, to be determined by the fit to the experimental data. This has to be contrasted to the usual XY-model description of the BKT transition, where μ/J_s is constrained to the value

$$\mu_{XY} = \frac{\pi^2}{2} J_s. \quad (16)$$

In general, the value of μ/J_s determines the temperature scale where significant deviations of J_s from the BCS temperature dependence $J^{BCS}(T)$ start to become visible. Indeed, even though free vortices only start to proliferate at T_{BKT} , if a significant density of vortex-antivortex pairs already exists below T_{BKT} , it can renormalize (*i.e.* suppress) the large-distance superfluid stiffness $J_s(T)$ with respect to its BCS behavior counterpart much before the BKT transition. In thin films of conventional superconductors it has been shown that this is the case.^{14,64} Here $\mu/J_s \simeq 1$, as expected in ordinary BCS superconductors, and the measured $J_s(T)$ deviates from the BCS behavior significantly before the universal jump (9) occurs. In contrast, it has been argued^{23,32} that, in cuprate superconductors, μ/J_s can even exceed the (large) value ≈ 4.9 in Eq. (16), where J_s is now the stiffness of a single layer (*i.e.* with $d_{BKT} = d_c$ in Eq. (1)). As we shall see below, this has relevant consequences for the determination of the effective transverse scale d_{BKT} for the BKT transition in a bulk material or in a thick film, as it is in our case.

A second effect to be taken into account in the analysis of the experiments is the presence of inhomogeneity of the local SC properties, which have been clearly shown to be relevant in underdoped cuprates by means of STM analysis of underdoped samples.^{72,73} Here we model^{14,32,64} the presence of inhomogeneities by assuming that the local BKT critical temperature has a finite distribution about the most probable value, represented by the curve labeled “Homogeneous” in Fig. 4. The main effect of the inhomogeneity is then to smear out the universal jump (9), the effect being larger for a wider probability distribution of the local T_{BKT} values. More details are given in Appendix B.

The results for the two samples $x = 0.07$ and $x = 0.08$ are shown in Fig. 4, and the fitting parameters are summarized in Table I. The BCS temperature dependence (13), shown in the figure with a dotted line, reproduces the data below the BKT transition very well, in particular for the $x = 0.08$ sample where more experimental points are available. Here the sample inhomogeneity is very small (width of the distribution $\delta/J_0 = 0.01$; see also

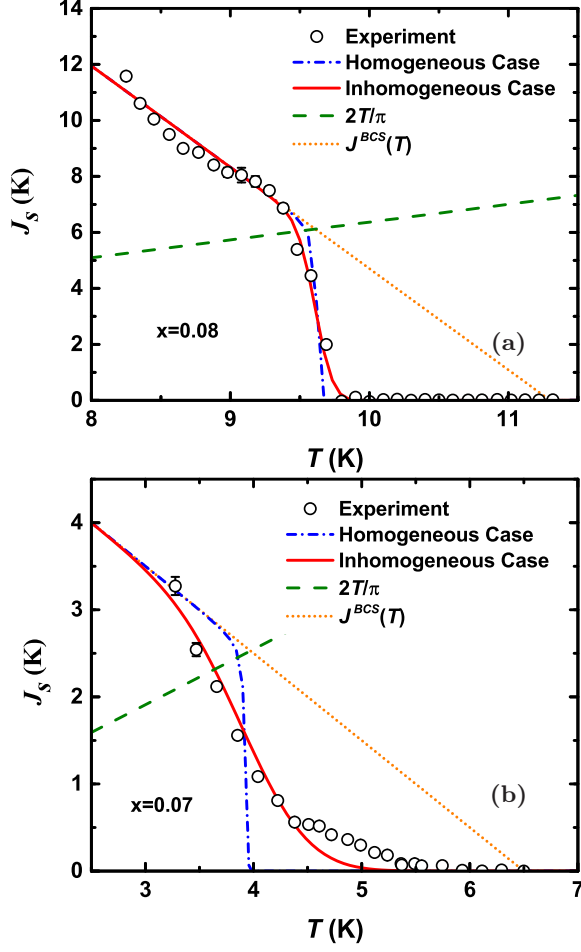


FIG. 4. Temperature dependence of the superfluid stiffness for the $x = 0.08$ (a) and $x = 0.07$ (b) samples: Comparison between the experiment and the theory, as described in the main text. The fitting parameters are listed in Table I.

TABLE I. Fitting parameters for Fig. 4.

doping	J_0 (K)	T_c (K)	T_{BKT} (K)	μ/J_s	δ/J_0	t_c	b_{theo}
0.07	6.5	6.5	4	6.3	0.1	0.625	2.02
0.08	41	11.3	9.7	7	0.01	0.16	1.15

Appendix B) and, accordingly, the homogeneous and inhomogeneous curves almost coincide, with a sharp downturn of $J_s(T)$ near T_{BKT} . T_{BKT} is defined here as the transition temperature for the homogeneous curve, which represents the most probable transition temperature for the sample. We note that, since we also included the effects of the finite size of the system, which lead to some rounding of the $J_s(T)$ jump before T_{BKT} , even in the homogeneous case we do not observe a strictly discontinuous jump as in Eq. (9), but J_s vanishes continuously over a temperature range of a few mK. For the $x = 0.07$ sample, the inhomogeneity is larger ($\delta/J_0 = 0.1$), as expected for a more underdoped sample, and this leads in

particular to a longer superfluid tail above T_{BKT} . In both samples, we extract a large value of the vortex-core energy, *i.e.* $\mu/J_s = 6 - 7$ or $\mu/\mu_{XY} \approx 1.4$. As explained above, this implies that the deviations of $J_s(T)$ from the BCS curve only occur near T_{BKT} . As a consequence, T_{BKT} can be very well estimated by using the universal relation (9) with $J_s(T_{BKT}^-)$ replaced by $J^{BCS}(T_{BKT}^-)$, *i.e.*

$$J^{BCS}(T_{BKT}) \simeq \frac{2T_{BKT}}{\pi} \Rightarrow t_c \simeq \frac{2T_c}{\pi J_0}, \quad (17)$$

which is in very good agreement with the t_c values listed in Table I, obtained by the RG results. It is apparent that the large separation between T_c and T_{BKT} in our samples is due to the presence of two concomitant effects in underdoped cuprate films: (i) the large mean-field critical temperature and (ii) the low superfluid stiffness, proportional to J_0 in Eq. (17), due to correlations.^{25,26} This has to be contrasted to conventional superconductors, where the BKT regime can only become visible when J_0 is suppressed by strong disorder, which also brings along unavoidable spurious effects connected to the inhomogeneity.^{14,33,64} In addition, in systems like NbN, it has been shown that $\mu/J_s \simeq 1$, so the deviations of $J_s(T)$ from the BCS behavior occur much *before* the intersection with the BKT line,^{14,64} making the approximate estimate (17) much less reliable.

Our finding of the large value of μ is an important result, since it confirms previous theoretical analysis^{23,32} in cuprates, and it allows us to understand the estimated value of $d_{BKT} \gtrsim d_c$ in our film, as discussed in Sec. II C. Since the measurements of $a(T)$ only access the areal superfluid stiffness (1) and thus do not allow for a separate determination of d_{BKT} and λ , the comparison of the experimental data and the theory shown in Fig. 4 has been done for the BKT transition in the pure 2D case. On the other hand, we also know that our films are comprised of $\sim 10^2$ layers, with a weak interlayer Josephson coupling between them. In this case, it has been proven by previous theoretical work^{23,32} that, when $\mu/\mu_{XY} > 1$, the BKT transition T_{BKT} moves away from the value expected for a single, isolated layer $T_{BKT}^{n=1}$. In particular, according to the analysis of Refs. 23 and 32, for the value of μ found above, one could expect that T_{BKT}^n is about 30% larger than $T_{BKT}^{n=1}$, corresponding to $d_{BKT} \simeq (2 - 3)d_c$. Indeed, by assuming $d_{BKT} \simeq 2d_c$ for the $x = 0.07$ sample, for example, one can easily estimate $T_{BKT} = T_{BKT}^{n=2} \simeq 1.3 T_{BKT}^{n=1}$ using the r.h.s. of Eq. (17). The value $d_{BKT} \simeq (2 - 3)d_c$ is consistent with the estimate based on the comparison to the penetration-depth measurements discussed in Sec. II C.

B. Paraconductivity

We note also that the value of μ extracted from the behavior of $J_s(T)$ is consistent with that obtained in Sec. II B from the analysis of the paraconductivity above

T_{BKT} , even though the fits presented there do not include the effect of SC inhomogeneities. Indeed, we can show that for our samples the inhomogeneity has a relatively minor effect on the determination of the parameters entering the paraconductivity fit. To show this, we analyze the paraconductivity above T_{BKT} by refining the analysis of Sec. II B with the inclusion of inhomogeneity.

We can describe the measured resistivity as

$$\frac{R}{R_n} = \left(1 + \frac{\Delta\sigma_{SCF}}{\sigma_n}\right)^{-1} = \left(1 + \left(\frac{2}{A} \sinh \frac{b}{\sqrt{t}}\right)^2\right)^{-1}. \quad (18)$$

In order to compare the theoretical predictions to a larger number of data points, in $\Delta\sigma_{SCF}(T) = \rho(T)^{-1} - \rho_n(T)^{-1}$, we approximate $\rho_n = 1/\sigma_n$ with a constant, zero-field value measured at $T \gg T_{BKT}$. Even though this procedure is less accurate far from T_{BKT} , this is not relevant for the discussion of the effects near T_{BKT} , where the SCFs contribution diverges. This is exemplified in Fig. 5, where paraconductivity obtained using this method is compared to that extracted from measurements in high magnetic fields (Sec. II B). Indeed, the exact determination of ρ_n becomes crucial only far from T_c , where $\Delta\sigma_{SCF}/\sigma_n$ becomes comparable to the difference ($\sim 10\%$) between its values obtained using those two methods.

For the $x = 0.07$ sample, we choose $R_n \equiv R(T = 20 \text{ K})$, where the SCFs contribution to conductivity is only a few per cent [Fig. 2(a)]. To account for the inhomogeneity, we follow the procedure discussed in Ref. 14, and outlined in Appendix B. We use the same distribution of local critical temperatures extracted from the analysis of $J_s(T)$ to generate a distribution of local resistivity values R_i/R_n described by Eq. (18) with the same local values T_{BKT}^i, T_c^i computed above. Thus, only A, b in Eq. (18) are the fitting parameters. The global resistance of the sample is then determined by the corresponding random-resistor-network problem by means of the effective-medium approximation. Once again, to elucidate the role of inhomogeneity, we compare the results for the homogeneous and inhomogeneous case. The ‘‘Homogenous’’ curve in Fig. 5 refers to the paraconductivity of a system with a single T_{BKT} and T_c realization, corresponding to the most probable value in the sample. Thus, this is the paraconductivity expected for a homogeneous system whose superfluid stiffness below T_{BKT} is described by the ‘‘Homogeneous’’ $J_s(T)$ curve in Fig. 4(b).

The results are shown in Fig. 5 for the parameters $A = 14$ and $b = 2.55$, which are in good agreement with the results of the analysis in Sec. II B. The differences are due to the effect of the inhomogeneity, which is known⁷⁴ to affect the slope of $R(T)$ above the transition. More importantly, $b = 2.55$ is very close to the theoretical value $b_{theo} = 2$ calculated from Eqs. (5), *i.e.*

$$b_{theo} = \frac{4}{\pi^2} \frac{\mu}{J_s} \sqrt{t_c}, \quad (19)$$

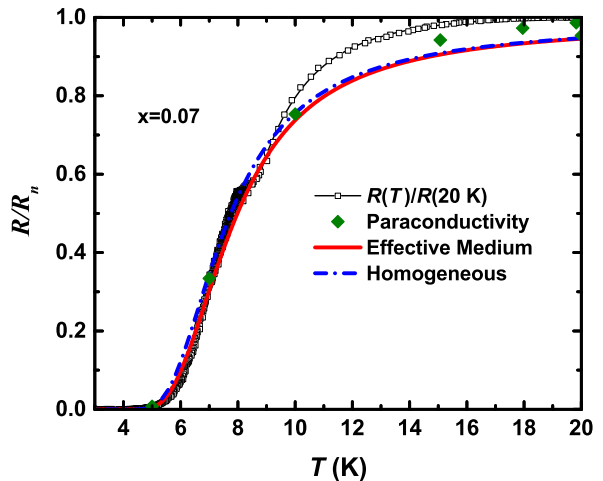


FIG. 5. Comparison between the $R(T)/R_n$ experimental data and the theoretical prediction obtained in the homogeneous or inhomogeneous case. In the latter case, $R(T)$ is obtained as solution of a random-resistor-network problem in the effective-medium approximation, as explained in Appendix B. Solid diamonds: Paraconductivity was extracted from measurements in high magnetic fields (Sec. II B).

by using the values of μ/J_s and t_c extracted from the analysis of the $I - V$ characteristics *below* T_{BKT} , and listed in Table I. The fit accurately reproduces the data up to $T \simeq 10 \text{ K}$, which is an extremely large range of SCFs, similar to Fig. 2(a). However, the BKT fluctuation regime only extends up to $T_c \approx 6.5 \text{ K}$ and, above it, ordinary AL-like Gaussian fluctuations are at play. Finally, we note that some deviations start to occur above $T \simeq 10 \text{ K}$. As we discuss in Appendix B, this effect has already been observed in several families of cuprates,^{41,42} and it can be interpreted as a signature of a pseudogap state above T_c .^{41,75}

IV. DISCUSSION

The analysis carried out in the previous Sections clearly demonstrates the occurrence of a BKT-like transition in our LSCO samples. This is confirmed both by the analysis of the paraconductivity above T_{BKT} and by the analysis of the superfluid stiffness below T_{BKT} , as extracted from the $I - V$ measurements. Even though our films are thick, in the sense that d is much larger than the SC coherence length, the possibility to see BKT physics is guaranteed by the layered nature of the system. As we discussed in Sec. I, a weakly-coupled layered superconductor is an ideal candidate for observing the BKT physics, since a layered structure ensures the best screening of the charged supercurrents. Indeed, in this case the interaction between vortices in each plane is logarithmic up to a scale $\Lambda_J \simeq \xi_0/\sqrt{J_\perp/J_\parallel}$ that grows as the stiffness anisotropy increases. While the behavior of J_\perp/J_\parallel as a function of doping in the LSCO family has

not been systematically explored, in other cuprates it has been shown to decrease significantly with underdoping,⁷⁶ along with a general suppression^{27,67} of J_{\parallel} due to correlation effects.^{25,26} Under these conditions, one could expect to identify signatures reminiscent of the typical 2D BKT physics, such as an almost discontinuous suppression of the superfluid stiffness, even in a layered *bulk* sample.^{19,20,23,24} On general grounds, the starting point of this reasoning is that, as demonstrated within several models^{19–24} the physics of a layered superconductor with a very weak interlayer coupling closely approaches that of an isolated 2D system. Indeed, even though the transition will ultimately have a 3D character, the 3D critical region is extremely reduced for weak interlayer Josephson coupling,^{19,21} and it could even be masked in the experiments due to finite-size effects or inhomogeneities of the type discussed in this manuscript.

Since in the BKT picture there exists a universal relation (9) between the transition temperature and the smallest superfluid stiffness beyond which vortex unbinding occurs, the idea that each layer is isolated can lead to the naive expectation that T_{BKT} is controlled by the stiffness of each isolated layer, *i.e.* the value (1) with $d_{BKT} = d_c$. However, as predicted theoretically,²³ this simple picture should be in part revised when the role of the vortex-core energy μ , controlling the vortex fugacity $g \sim e^{-\beta\mu}$, is taken into account. Indeed, in a layered BKT model the transition temperature is not controlled by the “bare” (*i.e.* short-distance) values of J_{\perp}/J_{\parallel} and of the vortex density g , but by their large-distance behavior. Both energy scales grow at large distances, with opposite consequences: the increasing of J_{\perp}/J_{\parallel} tries to keep the system superconducting, while the increase of g implies that vortices would like to proliferate making the system non-superconducting. While at some temperature g will ultimately win, the counter-action of the interlayer coupling can move T_{BKT} away from the temperature scale connected to the single-layer stiffness. Thus, the effective stiffness to be used in Eq. (9) has to be computed from the definition (1) with a transverse length scale d_{BKT} somewhat larger than d_c . In particular, as μ increases, the transition temperature moves farther away from the single-layer temperature scale.²³ The large value of the vortex-core energy obtained in our measurements suggests that, in strongly-underdoped LSCO samples, the relevant length scale controlling the BKT transition involves a few coupled layers, *i.e.* $d_{BKT} \gtrsim d_c$. This conclusion is in agreement with the estimate based on the measured superfluid stiffness (1), *i.e.* a combination d_{BKT}/λ^2 , and the comparison to λ measured in similar films.

These findings, based on the analysis of the superfluid stiffness below T_{BKT} , are confirmed by the analysis of the paraconductivity above it. In particular, we have shown that the SC fluctuations above T_{BKT} exhibit a BKT character near the transition, and then evolve into the ordinary Aslamazov-Larkin-type behavior expected for Gaussian (amplitude and phase) fluctuations.

We fitted the data with the well-known Halperin-Nelson formula,⁴⁴ which interpolates between the two regimes, by constraining the fitting parameters according to the theoretical expectations for them.⁶³ This procedure not only provides a consistency check of the validity of the BKT analysis, but it also allows us to confirm the estimate of the vortex-core energy extracted by the analysis of superfluid density. In agreement with previous findings in bulk cuprates,^{42,43,56} most of the fluctuation regime is dominated by Gaussian fluctuations with a marked 2D character, where the characteristic 2D unit is represented by a single layer, *i.e.* $d_{AL} = d_c$. It is worth stressing that this result is not in contradiction with the finding $d_{BKT} \gtrsim d_c$ for the BKT behavior. Indeed, in the case of Gaussian fluctuations, the dimensionality of the fluctuations is controlled only by the band-parameter anisotropy, *i.e.* the ratio t_{\perp}/t_{\parallel} between interlayer and intralayer hopping, respectively. When this ratio is small, as it is in cuprates, one can see 2D fluctuations over a broad temperature range.⁴⁷ The crossover to 3D behavior, expected in bulk materials, is here preceded by the vortex fluctuations, which drive the system towards a 2D BKT transition. Even if the transition will ultimately have a 3D character, we do not identify the crossover to 3D fluctuations. This is consistent with the fact that the 3D critical regime, especially above the transition,²¹ is extremely reduced in a weakly-coupled layered system and, in addition, it gets masked by inhomogeneous effects that are mostly relevant at the transition.

V. CONCLUSIONS

We have presented measurements of the in-plane transport properties of two strongly underdoped thick films of $\text{La}_{2-x}\text{Sr}_x\text{CuO}_4$. Our results have (i) established the occurrence of a BKT-like transition and (ii) identified the typical transverse length scale that defines the equivalent two-dimensional unit controlling the BKT signatures in this layered system.

The most striking signature of a vortex-driven phase transition emerges from the superfluid stiffness J_s , extracted from the exponent of the nonlinear $I - V$ characteristics across T_{BKT} . In both samples, we observe a rapid downturn of J_s reminiscent of the well-known universal jump expected in a 2D superconductor. A quantitative comparison with the theoretical predictions, which also include the effect of some unavoidable degree of inhomogeneity in the samples, strongly suggests a large energetic cost to create the vortex cores in the SC state. As a consequence, even though the interlayer Josephson coupling is weak, the vortex-pair unbinding occurs at a temperature larger than the one where each isolated layer would undergo the BKT transition.²³ In other words, the characteristic energy scale controlling the BKT properties corresponds to the superfluid stiffness of a few layers. These results are confirmed by the analysis of the paraconductivity above T_{BKT} . Thanks to the few-K dis-

tance between the BKT (T_{BKT}) and mean-field (T_c) critical temperatures, we can clearly see that an initial BKT regime of fluctuations crosses over to an extended regime of 2D Aslamazov-Larkin-type Gaussian fluctuations.

As we remarked above, the advantage of using highly underdoped thick films is that the intrinsically low value of the superfluid stiffness, due to the proximity to the Mott-insulating phase,^{25,26} allows us to achieve a large separation between T_{BKT} and T_c without simultaneously introducing a large disorder-driven inhomogeneity of the local SC properties. This has to be contrasted with the case of few-unit-cell thick films of cuprates,^{30,31} which are usually much more sensitive to disorder, so that the BKT jump of the superfluid stiffness is usually lost with underdoping.³¹ We note also that finite-frequency probes, such as the two-coil mutual inductance technique used in Ref. 31, can be potentially much more sensitive to disorder-induced inhomogeneity, as discussed recently within the context of films of conventional superconductors.³³ In contrast, the superfluid density extracted from the $I-V$ characteristics is a purely dc probe, and this can explain why we see a relatively sharp BKT jump even in our strongly underdoped samples. Whether these features are common to other families of cuprates is an interesting open question that certainly deserves further experimental and theoretical investigation.

ACKNOWLEDGMENTS

We thank A. T. Bollinger and I. Božović for the samples. We acknowledge V. Dobrosavljević for useful discussions. High-field ($H > 9$ T) measurements were performed in the National High Magnetic Field Laboratory (NHMFL) DC Field Facility. This work was partially supported by NSF Grants No. DMR-0905843, No. DMR-1307075, and the NHMFL through the NSF Cooperative Agreement No. DMR-1157490 and the State of Florida. L.B. acknowledges financial support by MIUR under projects FIRB-HybridNanoDev-RBFR1236VV, PRIN-RIDEIRON-2012X3YFZ2 and Premiali-2012 AB-NANOTECH.

Appendix A: Magnetoresistance

The H^2 dependence of the magnetoresistance is clearly observed at the highest T and H [Fig. 1(b)]. As the temperature is lowered and SCFs become stronger, the H^2 region gets pushed to higher fields and the curvature of the $\rho(H)$ dependence at high H , in the normal state, becomes less obvious. The same kind of behavior has been observed in other cuprates, *e.g.* in $\text{YBa}_2\text{Cu}_3\text{O}_{7-x}$ (Ref. 56) and in overdoped,^{55,57,58} underdoped,⁵⁵ and even non-superconducting^{48,55} LSCO very close to the onset of superconductivity.

In underdoped LSCO, it is well known^{55,77-79} that the resistivity at high H increases with decreasing T (*i.e.*

$d\rho/dT < 0$), as seen also in Fig. 1(a), reflecting the tendency towards an insulating ground state at high fields.⁵⁹ Nevertheless, deviations from Eq. (2) still provide a good estimate of $H'_c(T)$, as discussed below. While the precise reason for the applicability of Eq. (2) remains an open problem beyond the scope of this study, we note that, in the regime of interest, the system remains in the (poor) metallic regime, as $k_F l \gtrsim 1$ (k_F – Fermi wave vector, l – mean free path), *i.e.* the resistance per square per CuO_2 layer $\lesssim h/e^2$.

The quadratic dependence $H'_c(T) = H'_c(0)[1 - (T/T_2)^2]$ (see Fig. 2(a) inset) was found also in $\text{YBa}_2\text{Cu}_3\text{O}_{7-x}$ (Refs. 43 and 56) and overdoped LSCO (Ref. 58) giving us further confidence that the values of $H'_c(T)$ are reliable. Furthermore, the $H = 0$ onset temperature for SCFs, $T_2 = 29$ K, is consistent with the results from terahertz spectroscopy⁸⁰ obtained on similar films, and those determined from the onset of diamagnetism⁸¹ and the Nernst effect⁸² in LSCO crystals with similar $\rho(T)$ and T_c values. We also find that $\mu_0 H'_c(0) \simeq 15$ T is in agreement with the value of the upper critical field obtained from specific-heat measurements⁸³ on LSCO with a similar T_c . Therefore, even though the magnetoresistance method that we employed to determine H'_c and $\rho_n(H)$ has an inherent limitation in accuracy, we conclude that both the magnitude and the temperature dependence of the onset fields H'_c are fairly consistent with those from other types of studies. This consistency check confirms further that the observed onset of the H^2 magnetoresistance corresponds to the return to the normal state.

Appendix B: Renormalization-group analysis of the BKT transition for an inhomogeneous system

The BKT RG equations describe the large-distance behavior of the dimensionless quantities K and g introduced in Eqs. (14)-(15) above. They are given by^{3,4,17}

$$\frac{dK}{d\ell} = -K^2 g^2, \quad (\text{B1})$$

$$\frac{dg}{d\ell} = (2 - K)g, \quad (\text{B2})$$

where $\ell = \ln r/\xi_0$ is the rescaled length scale with respect to the short-distance cut-off for the problem, represented by the SC coherence length ξ_0 . The initial values of K and g are determined by the BCS value of the superfluid stiffness, Eq. (14), which includes only the temperature dependence due to quasiparticle excitations. The effect of vortices is accounted by the RG flow at large distances, so that the physical superfluid stiffness (1) is identified with the limiting value of K as one goes to large distances:⁶

$$J_s \equiv \frac{TK(\ell \rightarrow \infty)}{\pi}. \quad (\text{B3})$$

The basic idea of the RG equations is to look at the competition at large scales between the superfluid stiffness and the vortex fugacity. When $g \rightarrow 0$, it means that

single-vortex excitations are ruled out from the system, which then remains superconducting. Indeed, as one can see from Eqs. (B1) and (B2), when $g \rightarrow 0$, K goes to a constant and then J_s from Eq. (B3) is finite. If instead $g \rightarrow \infty$ at large distances, it means that vortices proliferate and drive the transition to the non-SC state, since $K \rightarrow 0$. The large-scale behavior depends on the initial values of the coupling constants K, g , which in turn depend on the temperature. The BKT transition temperature is defined as the highest value of T such that K flows to a finite value, so that J_s is finite. This occurs at the fixed point $K = 2, g = 0$, so that at the transition one always has $K(\ell = \infty) = 2$, corresponding to the universal relation (9) quoted above. By numerically solving Eqs. (B1)-(B2) at each temperature, while taking T_c and μ/J_{BCS} as free parameters in the initial value, we obtain the curve labeled as “Homogeneous” in Fig. 4, with the parameters reported in Table I.

To account for the presence of inhomogeneities, we follow the procedure discussed in previous publications for both conventional¹⁴ and cuprate³² superconductors. We assume that the BCS superfluid density is described by Eq. (13) with the initial value J_0^i randomly distributed according to a probability density $P(J_0^i)$ that we take, for instance, as Gaussian:

$$P(J_0^i) = \frac{1}{\sqrt{2\pi}\delta} \exp[-(J_0^i - J_0)^2/2\delta^2]. \quad (\text{B4})$$

In the homogeneous case, the Gaussian distribution has zero width and only the value J_0 is allowed. In this case, one obtains the $J_s(T)$ curve labeled as “Homogeneous” in Fig. 4, and the corresponding T_c, T_{BKT} are the ones reported in Table I. As we remarked in the text, we also add finite-size effects, by stopping the RG flow at the scale $\ell_{max} = L/\xi_0$ of the system size. As a consequence, even for the homogeneous case $J_s(T)$ does not display a real jump, but an extremely rapid downturn occurring over a few-mK temperature range. In the inhomogeneous case, for each J_0^i value distributed according to Eq. (B4), we rescale the corresponding BCS temperatures as $J_0^i/T_c^i = J_0/T_c$ and we compute $J_s^i(T)$ and the corresponding BKT temperatures T_{BKT}^i by the numerical solution of the RG equations (14)-(15) above. After obtaining this set of $J_s^i(T)$ curves, we compute the sample stiffness as the average one J_{av} , defined as

$$J_{av}(T) = \sum_i P(J_0^i) J_s^i(T). \quad (\text{B5})$$

When all the stiffness values $J_s^i(T)$ are different from zero, as it is the case at low temperatures, the average stiffness will be centered around the center of the Gaussian distribution (B4), so that it will coincide with $J^{BCS}(T)$. However, by approaching T_{BKT} defined by the average $J^{BCS}(T)$, not all the patches make the transition at the same temperature, so that the BKT jump is rounded and J_{av} remains finite above the average T_{BKT} , in agreement with the experiments. In this analysis, we

then have a second free parameter that is the width δ/J_0 of the Gaussian distribution (B4). However, all four parameters of the fit (average J_0 and T_c , ratio μ/J_s and δ/J_s) affect in a rather independent way the shape of the overall stiffness. Indeed, J_0 and T_c are essentially determined by the slope of the stiffness before the BKT transition, μ/J_s determines the location of the universal jump, whose smearing is controlled by δ . Thus, even though some flexibility is possible in the values of the parameters listed in Table I, these variations are expected to be within 10% – 20% of the quoted values.

The inhomogeneity also influences the paraconductivity above T_{BKT} . To show this, we proceed in analogy with Ref. 14 by mapping the spatial inhomogeneity of the sample in a random-resistor-network problem. In particular, we associate to each patch of initial stiffness value J_0^i a normalized resistance $\rho_i = R_i/R_n$ obtained from Eq. (18) by using the corresponding local values of T_c^i and T_{BKT}^i computed as outlined above. The overall sample normalized resistance $\rho = R/R_n$ is then calculated in the so-called effective-medium-theory (EMT) approximation,⁸⁴ where ρ is the solution of the self-consistent equation

$$\sum_i \frac{P_i(\rho - \rho_i)}{\rho + \rho_i} = 0. \quad (\text{B6})$$

Here P_i is the occurrence probability of each resistor, which coincides with the distribution function (B4) of the local J_0^i value used to compute the corresponding $\rho_i(T)$. The resulting $R(T) = \rho R_n$ is shown in Fig. 5, and it is compared to the one of the homogeneous case, *i.e.* the $R(T)$ curve obtained when only the most-probable J_0 value of the distribution (B4) is realized.

As we observed in Sec. III, for $T \gtrsim 10$ K the experimental paraconductivity saturates more rapidly than what is predicted by the HN interpolating formula. Since in this regime we are already exploring Gaussian fluctuations, such a failure is not correlated with the BKT character of the fluctuations, but it pertains instead to the regime of ordinary Cooper-pairs fluctuations. Interestingly, such behavior has been already observed in several families of cuprates,^{41,42} and it has been interpreted theoretically^{41,75} as an effect of the pseudogap. Indeed, by phenomenological modelling of the suppression in the electronic density of states characteristic of a preformed pseudogap, one can reproduce a faster decay of the Cooper-pairs correlation length $\xi(T)$ in Eq. (3) with respect to the standard AL prediction. Even though a detailed analysis of this issue is beyond the scope of the present manuscript, we nonetheless observed that a similar effect seems to be at play also in the case of our sample. To account for it within the HN interpolation scheme, we can for instance multiply the correlation length entering the paraconductivity formula (3) by a function suppressing it around a temperature T^* larger than T_c , such as

$$\xi(T) = \frac{2}{A} \sinh \frac{b}{\sqrt{t}} \exp(-(T/T^*)^4). \quad (\text{B7})$$

By introducing this correction factor in each normalized resistivity ρ_i appearing in Eq. (B6), we obtain the (homogeneous and inhomogeneous) curves displayed in Fig. 6. Here we used $T^* = 19$ K, that is, approximately the temperature where magnetoresistance saturates. As one can see in Fig. 6, our scheme now gives an excellent agreement with the experimental data up to $T \simeq 20$ K. In this high-temperature regime, the deviations of $R(T)$ from the magnetic-field extracted paraconductivity (symbols in Figs. 5 and 6) become sizeable, and the expression (B7) reproduces the latter points well.

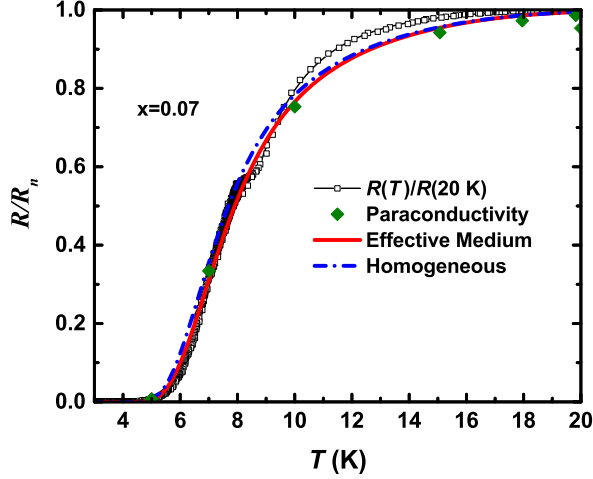


FIG. 6. Comparison between the $R(T)/R_n$ experimental data and the theoretical prediction obtained in the homogenous or inhomogeneous case for the modified HN correlation length (B7), including phenomenologically the pseudogap effect in the AL fluctuations. Solid diamonds: Paraconductivity extracted from measurements in high magnetic fields (Sec. II B).

-
- * Present address: Department of Physics, University of Texas at Dallas, Richardson, TX 75080, USA
[†] dragana@magnet.fsu.edu
¹ V.L. Berezinskii, Sov. Phys. JETP **34**, 610 (1972).
² J.M. Kosterlitz and D.J. Thouless, J. Phys. C **6**, 1181 (1973).
³ J.M. Kosterlitz, J. Phys. C **7**, 1046 (1974).
⁴ P. Minnhagen, Rev. Mod. Phys. **59**, 1001 (1987).
⁵ For a recent review see *40 Years of Berezinskii-Kosterlitz-Thouless Theory*, edited by Jorge V. Jos  (World Scientific, 2013).
⁶ D.R. Nelson and J.M. Kosterlitz, Phys. Rev. Lett. **39**, 1201 (1977).
⁷ D. McQueeney, G. Agnolet, and J. D. Reppy, Phys. Rev. Lett. **52**, 1325 (1984).
⁸ J. Pearl, Appl. Phys. Lett. **5**, 65 (1964).
⁹ A. T. Fiory, A. F. Hebard, and W. I. Glaberson, Phys. Rev. B **28**, 5075 (1983).
¹⁰ S. J. Turneaure, T. R. Lemberger, and J. M. Graybeal, Phys. Rev. Lett. **84**, 987 (2000).

- ¹¹ R.W. Crane, N. P. Armitage, A. Johansson, G. Sambandamurthy, D. Shahrar, and G. Gruner, Phys. Rev. B **75**, 094506 (2007).
¹² W. Liu, M. Kim, G. Sambandamurthy, and N.P. Armitage, Phys. Rev. B **84**, 024511 (2011).
¹³ A. Kamlapure, M. Mondal, M. Chand, A. Mishra, J. Jesudasan, V. Bagwe, L. Benfatto, V. Tripathi, and P. Raychaudhuri, Appl. Phys. Lett. **96**, 072509 (2010).
¹⁴ M. Mondal, S. Kumar, M. Chand, A. Kamlapure, G. Saraswat, G. Seibold, L. Benfatto, and P. Raychaudhuri, Phys. Rev. Lett. **107**, 217003 (2011).
¹⁵ Y.-H. Lin, J. Nelson, and A. M. Goldman, Phys. Rev. Lett. **109**, 017002 (2012).
¹⁶ S. Misra, L. Urban, M. Kim, G. Sambandamurthy, and A. Yazdani, Phys. Rev. Lett. **110**, 037002 (2013).
¹⁷ L. Benfatto, C. Castellani, and T. Giamarchi, book chapter in *40 Years of Berezinskii-Kosterlitz-Thouless Theory*, edited by Jorge V. Jos  (World Scientific, 2013).
¹⁸ G. Blatter, M. V. Feigel'man, V. B. Geshkenbein, A. I. Larkin, and V. M. Vinokur Rev. Mod. Phys. **66**, 1125

- (1994).
- 19 B. Chattopadhyay and S. R. Shenoy, Phys. Rev. Lett. **72**, 400 (1994).
 - 20 M. Friesen, Phys. Rev. B **51**, 632 (1995).
 - 21 S. W. Pierson, Phys. Rev. B **51**, 6663 (1995).
 - 22 P. Minnhagen and P. Olsson, Phys. Rev. B **44**, 4503 (1991).
 - 23 L. Benfatto, C. Castellani, and T. Giamarchi, Phys. Rev. Lett. **98**, 117008 (2007).
 - 24 K. S. Raman, V. Oganessian, and S. L. Sondhi, Phys. Rev. B **79**, 174528 (2009).
 - 25 V. J. Emery and S. A. Kivelson, Nature **374**, 434 (1995).
 - 26 P. A. Lee, N. Nagaosa, and X.-G. Wen, Rev. Mod. Phys. **78**, 17 (2006).
 - 27 D. M. Broun, W. A. Huttema, P. J. Turner, S. Ozcan, B. Morgan, R. Liang, W. N. Hardy, and D. A. Bonn, Phys. Rev. Lett. **99**, 237003 (2007).
 - 28 Y. L. Zuev, M.-S. Kim, and T. R. Lemberger, Phys. Rev. Lett. **95**, 137002 (2005).
 - 29 S. Kamal, D.A. Bonn, N. Goldenfeld, P. J. Hirschfeld, R. Liang, and W. N. Hardy Phys. Rev. Lett. **73**, 1845 (1994).
 - 30 I. Hetel, T. R. Lemberger, and M. Randeria, Nature Phys. **3**, 700 (2007).
 - 31 Jie Yong, M. J. Hinton, A. McCray, M. Randeria, M. Naamneh, A. Kanigel, and T. R. Lemberger, Phys. Rev. B **85**, 180507 (2012), and references therein.
 - 32 L. Benfatto, C. Castellani, and T. Giamarchi, Phys. Rev. B **77**, 100506(R) (2008).
 - 33 R. Ganguly, D. Chaudhuri, P. Raychaudhuri, and L. Benfatto, Phys. Rev. B **91**, 054514 (2015).
 - 34 P. C. E. Stamp, L. Forro, and C. Ayache, Phys. Rev. B **38**, 2847 (1988).
 - 35 N.-C. Yeh and C. C. Tsuei, Phys. Rev. B **39**, 9708 (1989).
 - 36 D. P. Norton and D. H. Lowndes, Phys. Rev. B **48**, 6460 (1993).
 - 37 N. Cotón, M. V. Ramallo, and F. Vidal, arXiv:1309.5910.
 - 38 S. Dietrich, W. Mayer, S. Byrnes, S. Vitkalov, A. Sergeev, A. T. Bollinger, and I. Božović, Phys. Rev. B **91**, 060506 (2015).
 - 39 G. Balestrino, A. Nigro, R. Vaglio, and M. Marinelli, Phys. Rev. B **39**, 12264 (1989).
 - 40 G. Balestrino, M. Marinelli, E. Milani, L. Reggiani, R. Vaglio, and A. A. Varlamov, Phys. Rev. B **46**, 14919 (1992).
 - 41 S. Caprara, M. Grilli, B. Leridon and J. Lesueur, Phys. Rev. B **72**, 104509 (2005).
 - 42 B. Leridon, J. Vanacken, T. Wambecq, and V. V. Moshchalkov, Phys. Rev. B **76**, 012503 (2007).
 - 43 F. Rullier-Albenque, H. Alloul, and G. Rikken, Phys. Rev. B **84**, 014522 (2011).
 - 44 B.I. Halperin and D.R. Nelson, J. Low Temp. Phys. **36**, 599 (1979).
 - 45 L. G. Aslamazov and A. I. Larkin, Phys. Lett. **26A**, 238 (1968).
 - 46 L. G. Aslamazov and A. I. Larkin, Sov. Phys. Solid State **10**, 875 (1968).
 - 47 A. Larkin and A. Varlamov, *Theory of Fluctuations in Superconductors* (Oxford University Press, Oxford, 2009).
 - 48 X. Shi, G. Logvenov, A. T. Bollinger, I. Božović, C. Panagopoulos, and D. Popović, Nature Mater. **12**, 47 (2013).
 - 49 See <http://www.keithley.com> for Keithley Instruments, Inc., 28775 Aurora Road, Cleveland, Ohio 44139.
 - 50 M. C. Sullivan, T. Frederiksen, J. M. Repaci, D. R. Strachan, R. A. Ott, and C. J. Lobb, Phys. Rev. B **70**, 140503(R) (2004).
 - 51 A. Lacerda, J. P. Rodriguez, M. F. Hundley, Z. Fisk, P. C. Canfield, J. D. Thompson, and S. W. Cheong, Phys. Rev. B **49**, 9097 (1994).
 - 52 J. M. Harris, Y. F. Yan, P. Matl, N. P. Ong, P. W. Anderson, T. Kimura, and K. Kitazawa, Phys. Rev. Lett. **75**, 1391 (1995).
 - 53 T. Kimura, S. Miyasaka, H. Takagi, K. Tamasaku, H. Eisaki, S. Uchida, K. Kitazawa, M. Hiroi, M. Sera, and N. Kobayashi, Phys. Rev. B **53**, 8733 (1996).
 - 54 Y. Ando and K. Segawa, Phys. Rev. Lett. **88**, 167005 (2002).
 - 55 J. Vanacken, L. Weckhuysen, T. Wambecq, V. Mashkautsan, P. Wagner, and V. V. Moshchalkov, Physica C **404**, 385 (2004).
 - 56 F. Rullier-Albenque, H. Alloul, C. Proust, P. Lejay, A. Forget, and D. Colson, Phys. Rev. Lett. **99**, 027003 (2007).
 - 57 R. A. Cooper, Y. Wang, B. Vignolle, O. J. Lipscombe, S. M. Hayden, Y. Tanabe, T. Adachi, Y. Koike, M. Nohara, H. Takagi, C. Proust, and N. E. Hussey, Science **323**, 603 (2009).
 - 58 P. M. C. Rourke, I. Mouzopoulou, X. Xu, C. Panagopoulos, Y. Wang, B. Vignolle, C. Proust, E. V. Kurganova, U. Zeitler, Y. Tanabe, T. Adachi, Y. Koike, and N. E. Hussey, Nature Phys. **7**, 455 (2011).
 - 59 X. Shi, P. V. Lin, T. Sasagawa, V. Dobrosavljević, and D. Popović, Nature Phys. **10**, 437 (2014).
 - 60 M. K. Chan, M. J. Veit, C. J. Dorow, Y. Ge, Y. Li, W. Tabis, Y. Tang, X. Zhao, N. Barišić, and M. Greven, Phys. Rev. Lett. **113**, 177005 (2014).
 - 61 A. B. Pippard, *Magnetoresistance in Metals* (Cambridge Univ. Press, 1989).
 - 62 W. Lang, G. Heine, W. Kula, and R. Sobolewski, Phys. Rev. B **51**, 9180 (1995).
 - 63 L. Benfatto, C. Castellani, and T. Giamarchi, Phys. Rev. B **80**, 214506 (2009).
 - 64 J. Yong, T. R. Lemberger, L. Benfatto, K. Ilin, and M. Siegel, Phys. Rev. B **87**, 184505 (2013).
 - 65 N. Reyren, S. Thiel, A. D. Caviglia, L. Fitting Kourkoutis, G. Hammerl, C. Richter, C. W. Schneider, T. Kopp, A.-S. Rüetschi, D. Jaccard, M. Gabay, D. A. Muller, J.-M. Triscone, and J. Mannhart, Science **317**, 1196 (2007).
 - 66 T. I. Baturina, S. V. Postolova, A. Yu. Mironov, A. Glatz, M. R. Baklanov, and V. M. Vinokur, EPL **97**, 17012 (2012).
 - 67 J.-P. Locquet, Y. Jaccard, A. Cretton, E. J. Williams, F. Arrouy, E. Mächler, T. Schneider, Ø. Fischer, and P. Martinoli, Phys. Rev. B **54**, 7481 (1996).
 - 68 H. Weber, M. Wallin, and H. J. Jensen, Phys. Rev. B **53**, 8566 (1996).
 - 69 S. W. Pierson, M. Friesen, S. M. Ammirata, J. C. Hunnicutt, and LeRoy A. Gorham, Phys. Rev. B **60**, 1309 (1999).
 - 70 A. Gurevich and V. M. Vinokur, Phys. Rev. Lett. **100**, 227007 (2008).
 - 71 A. Andersson and J. Lidmar, Phys. Rev. B **87**, 224506 (2013).
 - 72 Ø. Fischer, M. Kugler, I. Maggio-Aprile, C. Berthod, and C. Renner, Rev. Mod. Phys. **79**, 353 (2007).
 - 73 C. V. Parker, A. Pushp, A. N. Pasupathy, K. K. Gomes, J. Wen, Z. Xu, S. Ono, G. Gu, and A. Yazdani, Phys. Rev. Lett. **104**, 117001 (2010).
 - 74 S. Caprara, M. Grilli, L. Benfatto, and C. Castellani, Phys. Rev. B **84**, 014514 (2011).
 - 75 A. Levchenko, M. R. Norman, and A. A. Varlamov, Phys.

- Rev. B **83**, 020506 (2011).
- ⁷⁶ A. Hosseini, D. M. Broun, D. E. Sheehy, T. P. Davis, M. Franz, W. N. Hardy, Ruixing Liang, and D. A. Bonn, Phys. Rev. Lett. **93**, 107003 (2004).
- ⁷⁷ Y. Ando, G. S. Boebinger, A. Passner, T. Kimura, and K. Kishio, Phys. Rev. Lett. **75**, 4662 (1995).
- ⁷⁸ K. Karpińska, A. Malinowski, M. Z. Cieplak, S. Guha, S. Gershman, G. Kotliar, T. Skośkiewicz, W. Plesiewicz, M. Berkowski, and P. Lindenfild, Phys. Rev. Lett. **77**, 3033 (1996).
- ⁷⁹ G. S. Boebinger, Y. Ando, A. Passner, T. Kimura, M. Okuya, J. Shimoyama, K. Kishio, K. Tamasaku, N. Ichikawa, and S. Uchida, Phys. Rev. Lett. **77**, 5417 (1996).
- ⁸⁰ L. S. Bilbro, R. Valdés Aguilar, G. Logvenov, O. Pelleg, I. Božović, and N. P. Armitage, Nature Phys. **7**, 298 (2011).
- ⁸¹ L. Li, Y. Wang, S. Komiya, S. Ono, Y. Ando, G. D. Gu, and N. P. Ong, Phys. Rev. B **81**, 054510 (2010).
- ⁸² Y. Wang, Z. A. Xu, T. Kakeshita, S. Uchida, S. Ono, Y. Ando, and N. P. Ong, Phys. Rev. B **64**, 224519 (2001).
- ⁸³ Y. Wang and H-H. Wen, Europhys. Lett. **81**, 57007 (2008).
- ⁸⁴ S. Kirkpatrick, Rev. Mod. Phys. **45**, 574 (1973).